AIChE

# Constant Number Monte Carlo Simulation of Population Balances with Multiple Growth Mechanisms

**Samira Khalili, Yulan Lin, Antonios Armaou, and Themis Matsoukas**
Dept. of Chemical Engineering, Pennsylvania State University, PA 16802

*DOI 10.1002/aic.12233*
*Published online April 12, 2010 in Wiley Online Library (wileyonlinelibrary.com).*

*We present a complete simulation scheme for particulate processes based on the constant number Monte Carlo methodology. Specifically, the proposed scheme can be applied towards the solution of population balances that include nucleation, coagulation and surface deposition, coupled to chemical reactions. The synthesis of titania ($TiO_2$) by flame oxidation of $TiCl_4$ is employed as a comparison basis of the relative advantages and weaknesses of Monte Carlo against more classical numerical approaches.* © 2010 American Institute of Chemical Engineers *AIChE J,* 56: 3137–3145, 2010
*Keywords: constant number Monte Carlo, population balance, titania synthesis*

## Introduction

Modeling of particulate processes has reached the point where the use of population balances is quite common at the research level. At the same time, the development and refinement of solution methodologies for population balance problems continues vigorously in all areas of particle science including colloids and polymers[1–3], aerosols[4–7], and powders.[8] Such population models have been extensively used to design and control chemical and biological processes;[9–12] the reader may refer to the excellent reviews[13,14] and references therein.

The need for improved numerical tools arises from the fact that the population balance equation (PBE) generally contains both derivative and integral terms of the size distribution, which in turn may exhibit discontinuities due to appearance or disappearance of discrete sizes (for example, nucleation or dissolution). Monte Carlo (MC) methods circumvent some of these difficulties.[15] In particular, the MC treatment of aggregation and break up is straightforward and involves none of the numerical difficulties encountered by standard integration techniques that are based in some type of discretization of the size distribution. Indeed, this is the natural advantage of MC, whose discrete nature is well suited to handle discrete events between finite numbers of particles. Not all particulate mechanisms share these characteristics, however. A case in point is growth by surface deposition, a single-particle process in which growth takes place via a process that is continuous in time. Other examples of continuous processes are particle dissolution, which can be viewed as the reverse process to surface deposition, particle restructuring (e.g., sintering and consolidation of porous particles), or presence of chemical reactions that are coupled to the particles, for example, via nucleation or surface reaction. These mechanisms can be incorporated easily into standard discretization methods but require special handling in MC. Therefore, discretization techniques and MC methods stand at opposite ends with respect to ease of use in population balances, depending on the mechanisms that are present. Since many particulate processes of industrial interest involve multiple mechanisms simultaneously, often coupled to a set of chemical reactions, the numerical solution of the PBE is no longer a straightforward task, regardless of which methodology is chosen.

The purpose of this article is to present a complete MC simulation environment for the solution of a population

Correspondence concerning this article should be addressed to T. Matsoukas at matsoukas@engr.psu.edu.

balance model that includes nucleation, coagulation and surface deposition, coupled to a chemical reaction. We have chosen the synthesis of titania ($TiO_2$) by flame oxidation of $TiCl_4$ as the process of interest. This is a system of industrial importance that has been studied experimentally and for which kinetic information is available. It is also a system that has been studied numerically by Spicer et al. using a variety of discretization techniques.[16–20] This provides us both with a means of validating the MC methodology, but also with a basis to compare the relative advantages and weaknesses of MC against more classical numerical approaches. The article is organized as follows. We first outline the chemical model implemented in this work. We then show explicitly how the kinetic information is converted into dimensionless form appropriate for the calculation of event probabilities. Subsequently, we describe the set up of constant-Number MC and show how all relevant quantities are computed in the simulation. Finally, we present and discuss the results of this approach.

### *Population balance model*

*Kinetics.* The kinetic model used in this study is the same previously used by Spicer et al. (see Figure 1). $TiCl_4$ is consumed via a reaction that is overall first order in the concentration of $TiCl_4$ with rate constant

$$k_0 = 8.26 \times 10^4 \exp\left(\frac{-10681}{T}\right) \quad (1/\mathrm{s}) \tag{1}$$

with $T$ in K. The overall decomposition rate reflects the combined effect of homogeneous gas-phase nucleation, which is taken to be first order in the concentration of $TiCl_4$ with rate constant $k_N$, and oxidation of $TiCl_4$ on the aerosol surface:

$$k_0 = k_N + k_D A \tag{2}$$

Here, $A$ is the surface area of the aerosol per unit volume ($m^2/m^3$), $k_N$ is the rate constant for homogeneous nucleation (1/s) and $k_D$ is rate constant for surface deposition (m/s). The rate constant for surface deposition is given by Spicer et al,

$$k_D = 49.0 \exp\left(\frac{-8993}{T}\right) \quad (\mathrm{m/s}) \tag{3}$$

while the nucleation rate is calculated from Eq. 2 and the known values of $k_0$, $k_D$.

The reaction zone is modeled as a plug flow reactor with no radial gradients. For simplicity, the reactor is also assumed isothermal, although this assumption can be easily relaxed if the temperature profile is known. Under these conditions the system is treated as a well-mixed batch process in which time represents the residence time in the reaction zone.

The above constants are needed in the balance of unreacted $TiCl_4$, where the time evolution of $C_0$ (molecules/$m^3$) is given by:

$$\frac{dC_0}{dt} = -(k_N + Ak_D)C_0 \tag{4}$$

where $A$ is expressed in $m^2/m^3$. The coagulation rate is calculated using Fuchs' formula which interpolates between the kinetic and the continuum regimes[21] (see the Appendix). For simplicity we assume that upon coagulation, particles instantaneously coalesce into a sphere. This assumption may be relaxed to include a finite rate of coalescence (sintering).

*Event rates.* We begin by defining the events that will be simulated by MC and their probabilities. The main events in the process described above are: (i) nucleation of new particles; (ii) coagulation of particles; and (iii) surface deposition. These events will further be refined by selecting the specific particle(s) that participate in the implementation of each of the above events (discussed in the next section). In this section we derive expressions for the total rate of these events in terms of variables that are accessible to the simulation. All results are presented in dimensionless form based on a characteristic concentration $C_*$ ($m^{-3}$), a characteristic mass $M_*$ (kg) and a characteristic time, $t_*$ (s). In the simulation, $t_*$ is selected among the characteristic times scales of the various rate processes (nucleation, surface growth, or coagulation), to be defined later. Until then we treat $t_*$ as a constant. We choose $C_*$ to be the initial concentration of $TiCl_4$ in the feed, and $M_*$ to be the mass of a $TiO_2$ species.

The characteristic diameter $d_*$, and surface area $A_*$ are defined as follows

$$d_* = (6M_*/\pi\rho)^{1/3} \tag{5}$$

$$A_* = \pi d_*^2 \tag{6}$$

where $\rho$ is the density of titania. Finally, the specific rate $R_e$ of event e (nucleation, coagulation or surface deposition) is made dimensionless as follows:

$$r_e = \frac{R_e t_*}{C_*}. \tag{7}$$

Table 1 summarizes the definitions of the various dimensionless quantities.

*Nucleation.* The rate of nucleation is

$$R_N = k_N C_0 \tag{8}$$

where $C_0$ is the concentration of unreacted $TiCl_4$ in $m^{-3}$. We express the rate in dimensionless form $r_N = R_N t_*/C_*$ where $t_*$, $C_*$, are a characteristic time and characteristic concentration, and which are to be defined later. The dimensionless rate $r_N$ is

$$r_N = \frac{c_0}{\tau_N/t_*} \tag{9}$$

where $c_0 = C_0/C_*$ is the dimensionless concentration of unreacted $TiCl_4$, and $\tau_N = 1/k_N$ is the time scale for nucleation. We note that nucleation adds a mass $M_N$ to the system, equal to the mass of the nucleus.

*Surface deposition.* For the purposes of the simulation we define a surface deposition event as the deposition of mass $M_D$ onto a particle. Accordingly, the rate of deposition events is

$$R_D = k_D A \frac{M_0}{M_D} \tag{10}$$

where $M_0$ is the mass of a $TiO_2$ cluster. The total surface area is expressed as

**Table 1. Characteristic and Dimensionless Variables**

| | Dimensional Variables |
|---|---|
| $d_*$ | $0.42 \times 10^{-9}$ m |
| $M_* = \rho\pi d_*^3/6$ | $1.5517 \times 10^{-25}$ kg |
| $A_* = \pi d_*^2$ | $5.54 \times 10^{-19}$ m$^2$ |
| $C_*$ | Initial concentration of $TiCl_4$, 1/m$^3$ |
| | **Dimensionless Variables** |
| $c_0 = C_0/C_*$ | Concentration of $TiCl_4$ |
| $c_p = C_p/C_*$ | Number concentration of particles |
| $c_m = C_M/C_*M_*$ | Mass concentration of particles |
| $x = d/d_*$ | Particle size |
| $a = A/A_*$ | Concentration of total surface area |
| $\bar{a} = a/c_p$ | Average surface area per particle |
| $v = x^3$ | Dimensionless particle mass |
| $v_N = 1$ | Dimensionless mass of $TiO_2$ nucleus |
| $v_D = M_D/M_*$ | Dimensionless mass deposited per event |
| $r_e = R_e\, C_*/t_*$ | Rate of event $e$ = {nucleation, surface deposition, coagulation} |
| $\tau_N$ | Time constant of nucleation |
| $\tau_D$ | Time constant of surface deposition |
| $\tau_C$ | Time constant of coagulation |

$$A = \bar{A} C_p \tag{11}$$

where $\overline{A}$ is the surface per particle (number average surface area) and $C_p$ is the total number concentration of particles. The mean area is calculated during the simulation assuming the particles to be spherical: $\overline{A}/A_* = (\overline{x})^{2/3}$, where $x$ is the dimensionless particle mass. Combining the above equations and expressing all variables in dimensionless form, we obtain

$$r_D = \frac{\bar{a} c_0\, c_p}{\tau_D/t_*} \tag{12}$$

where $\bar{a}$ is the dimensionless average area per particle, $c_p$ is the dimensionless particle concentration and $\tau_D$ is the time scale for surface deposition, defined as

$$\tau_D = \frac{M_D}{M_0 k_D C_* A_*} \tag{13}$$

*Coagulation.* The total coagulation rate is

$$R_C = \frac{\langle K_{12}\rangle C_P^2}{2} \tag{14}$$

where $\langle K_{12}\rangle$ is the average kernel between all particles in the population.[22,23] Next, we write the coagulation kernel in the form $K_{12} = K_C k_{12}$, where $K_C$ is the dimensional part of the kernel (m$^2$/s), and $k_{12}$ is a dimensionless function of particle size (see Appendix for details). In dimensionless form, the coagulation rate is

$$r_C = \frac{\langle k_{12}\rangle c_p^2}{\tau_C/t_*} \tag{15}$$

where $\tau_C$ is the time scale for coagulation and is given by

$$\tau_C = 2/K_C C_* \tag{16}$$

*Characteristic times.* The nucleation characteristic time is calculated as $\tau_N = 1/k_N$ with $k_N$ and obtained from Eq. 2 and $k_D$ from Eq. 13:

$$\tau_N = \frac{1}{k_0 - v_D c_p \bar{a}/\tau_D} \tag{17}$$

Note that the nucleation time is not constant but depends on the concentration of surface area (expressed via $v_D c_p \bar{a}$), which varies in time. The characteristic time for deposition is calculated from Eq. 13, which we rewrite as

$$\tau_D = v_D/k_D C_* A_*, \tag{18}$$

where $v_D = M_D/M_0$ is the dimensionless mass of the depositing species during surface deposition. The simulation begins with $v_D = 1$ (i.e., the depositing unit is one molecule) but the value is increased at later times in order to speed up the calculation. The characteristic time for coagulation is calculated from Eq. 16.

### *Implementation of constant-number MC*

In constant-Number Monte Carlo (cNMC)[22,23] we utilize a simulation box that contains a constant number $N$ to represent the actual concentration of particles. The basic algorithm is summarized as follows. During each step, we select the event to implement (nucleation, surface deposition, or coagulation) and produce a corresponding change in the simulation box. If the number of particles changes as a result of the event, an additional step is performed to restore the size of the box to $N$. Following the implementation of an event, time and concentrations are updated and the above steps are repeated. Below we discuss each of these steps in detail.

*Implementation of events.* Each MC step represents the realization of a single event (nucleation, surface deposition, coagulation) and advances time by the mean inter-event interval based on the the total rate of events:

$$\delta t = \frac{1}{r_N + r_D + r_C} \tag{19}$$

Events are implemented with probabilities proportional to the rate of that event:

$$P_e = \frac{r_e}{r_N + r_D + r_C} \tag{20}$$

where subscript $e$ represents nucleation, deposition or coagulation. The rates and the characteristic times of the events are summarized in Table 2. Events are implemented as follows:

1. Nucleation: a particle nucleus ($v = 1$) is added to the simulation box; a randomly selected particle is deleted from

**Table 2. Rate and Characteristic Time of Events**

| Event | Rate (1/s) | Characteristic Time |
|---|---|---|
| Nucleation | $r_N = \dfrac{c_0}{\tau_N}$ | $\tau_N = \dfrac{1}{k_0 - c_p v_D \bar{a}/\tau_D}$ |
| Surface deposition | $r_D = \dfrac{\bar{a} c_0\, c_p}{\tau_D}$ | $\tau_D = \dfrac{v_D}{k_D C_* A_*}$ |
| Coagulation | $r_C = \dfrac{\langle k_{12}\rangle c_p^2}{\tau_C}$ | $\tau_C = \dfrac{1}{K_C C_*}$ |

the simulation box in order to keep the number of particles constant.

2. Deposition: a particle $i$ is chosen with probability $P_i$ proportional to the deposition rate for that particle. Since the deposition rate is proportional to the particle area, $a_i$, all other factors being constant, this probability is $P_i = a_i/a$, where $a$ is the total area in the simulation box. Once a particle is chosen, its mass is incremented by $v_D$.

3. Coagulation: a pair $(i, j)$ of particles is chosen with probability proportional to the coagulation rate of the pair; since this rate is proportional to $k_{ij}$, all other factors being constant, this probability is calculated as

$$P_c = \frac{k_{ij}}{k_{max}} \tag{21}$$

where $k_{max}$ is the maximum value for the coagulation kernel in the simulation box. Once a pair is selected with masses $v_i$, $v_j$, respectively, it is erased from the simulation box and a new particle is formed with mass $v_i + v_j$. A randomly selected particle is replicated and its copy is placed in the simulation box so that the number of simulation particles is always $N$.

The rate (and probability) of coagulation requires the calculation of the average coagulation kernel over all pairs in the simulation box:

$$\langle k_{ij} \rangle = 2 \frac{\sum_{i=1}^{N-1} \sum_{j=1+1}^{N} k_{ij}}{N(N-1)}. \tag{22}$$

This computation scales as $N^2$ with the number of simulation particles and becomes more expensive if the mathematical form of the kernel is algebraically involved, as in the case of the Fuchs kernel (see Appendix). In order to accelerate the execution, we adopt a sampling approach as follows; when coagulation is the chosen event, we keep track of the value of $k_{ij}$ of all pairs sampled before a suitable pair is found and estimate $\langle k_{ij} \rangle$ as the average of this sample.

The above steps produce a sample of the particle population of constant size $N$ that evolves in time in accordance with the rates of the processes in the reactor that is being simulated. All metrics of the population, including average mass, $\bar{v}$, average area, $\bar{a}$, total area $a$, etc. are calculated directly from the sample of particles.

*Concentrations.* In cNMC, a simulation box with constant number of particles represents a system in which the actual particle concentration varies with time. It is important then to establish the connection between concentrations and changes in the simulation box properly. To make this connection, we note that before the implementation of an event the simulation box contains total mass $M = N\bar{v}$ that represents a mass concentration $c_M$. If the event adds mass $\delta v_e$ to the simulation box, the corresponding change in $c_M$ is

$$\delta c_M = \frac{c_M}{N\bar{v}} \delta v_e \tag{23}$$

The value of $\delta v_e$ depends on the event and for the mechanisms we consider here the possible values are:

$$\delta v_e = \begin{cases} v_N & \text{if nucleation} \\ v_D & \text{if deposition} \\ 0 & \text{if coagulation} \end{cases} \tag{24}$$

The corresponding change in the concentration of unreacted $TiCl_4$ is

$$\delta c_0 = -\delta c_M = -\frac{c_M}{N\bar{v}} \delta v_e \tag{25}$$

Finally, the particle number concentration after the implementation of an event is obtained from its relationship to $\bar{v}$ and $c_M$:

$$c_P = \frac{c_M}{\bar{v}} \tag{26}$$

Equations 19, 23, 25, and 26 summarize the increment for time, mass and number concentration of particles, and concentration of chemical precursor, based on the changes applied to the simulation box. Although alternative methods can be used to update concentrations, the method presented here is more accurate, as discussed in Ref. 23.

## Results and Discussion

We performed calculations at 1800 K and 1400 K with initial moL fraction of $TiCl_4$ 0.1 and 0.5 (in all cases $P =$ 1.013 bar). To compare with the work of Spicer et al.,[16] we run simulations both with and without surface deposition. The cases are summarized in Table 3 along with the corresponding characteristic times. Since the results are similar to the results of Spicer et al. at both temperatures, we only present graphs from the calculations at 1800 K. Figure 2 shows the concentration of $TiCl_4$ as a function of time for $T = 1800$ K and $x_{TiCl_4} = 0{:}1$. In the absence of surface

**Table 3. Parameters for Simulations**

| Deposition | $T$ (K) | $P$ (bar) | $x_{TiCl_4}$ | $\tau_N$ (s) | $\tau_D$ (s) | $\tau_C$ (s) | Run Time* (min) |
|---|---|---|---|---|---|---|---|
| Yes | 1800 | 1.013 | 0.1 | $4.57 \times 10^{-3\dagger}$ | $1.34 \times 10^{-5\ddagger}$ | $6.66 \times 10^{-9}$ | 18 |
| No | 1800 | 1.013 | 0.1 | $4.57 \times 10^{-3}$ | – | $6.66 \times 10^{-9}$ | 77 |
| Yes | 1400 | 1.013 | 0.1 | $2.49 \times 10^{-2}$ | $4.33 \times 10^{-5\ddagger}$ | $5.87 \times 10^{-9}$ | 26 |
| No | 1400 | 1.013 | 0.1 | $2.49 \times 10^{-2}$ | – | $5.87 \times 10^{-9}$ | 316 |
| Yes | 1400 | 1.013 | 0.5 | $2.49 \times 10^{-2\dagger}$ | $8.66 \times 10^{-6\ddagger}$ | $1.17 \times 10^{-10}$ | 69 |
| No | 1400 | 1.013 | 0.5 | $2.49 \times 10^{-2}$ | – | $1.17 \times 10^{-10}$ | 961 |

*Using MATLAB with $N = 1000$ particles on a single Dual core 2.4 GHz AMD Opteron with 8 GB of ECC RAM node.
†In the presence of surface deposition $\tau_N$ varies with time; value in table refers to $t = 0$.
‡From Eq. 18 with $v_D = 1$; $v_D$ is increased during simulation.

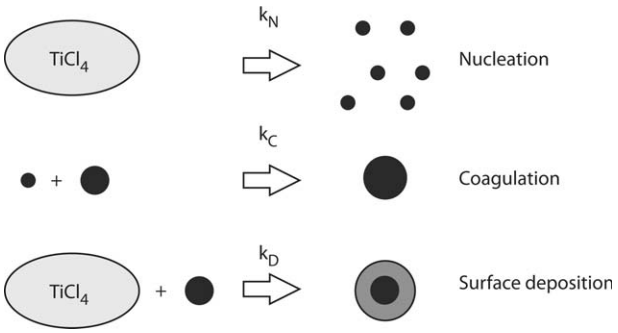


**Figure 1. Schematic representation of growth mechanisms.**

deposition, the nucleation rate is first order in the concentration of titanium tetrachloride with $\tau_N = 4.57 \times 10^{-3}$ s and as we see, the simulation results show excellent agreement with the expected exponential decay. When surface deposition is included, the decay of the monomer is faster, since it is depleted via both nucleation and deposition.

The evolution of the particle diameter, which we calculate as $d_p = (\overline{d^3})^{1/3}$, is shown in Figure 3. Both with and without surface deposition, the results are in very good agreement with the results of Spicer et al.[16] It is worth noting that the agreement extends to the small dip in size observed around $t \approx 0.02$ s and which is due to a second nucleation burst that introduces a significant amount of small particles. After all the tetrachloride is consumed ($t \approx 0.1$ s) the process is dominated by coagulation only and the particle diameter converges onto the a universal coagulation line.

The complete size distributions are shown in Figure 4 (with surface deposition) and Figure 5 (without deposition). The size distribution, $f(d)$, is defined as

$$f(d) = \frac{c_P}{N}\frac{\delta N(d)}{\delta d} \tag{27}$$

where $\delta N(d)$ is the number of particles in the size range $\delta d$, $N$ is the total number of particles in the simulation box and $c_P$ is

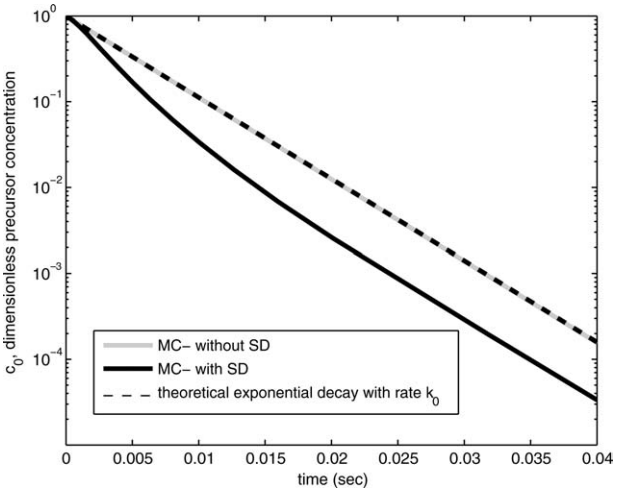


**Figure 2. Concentration of $TiCl_4$ as function of time ($T$ = 1800 K, $x_{TiCl_4}$ = 0.1).**

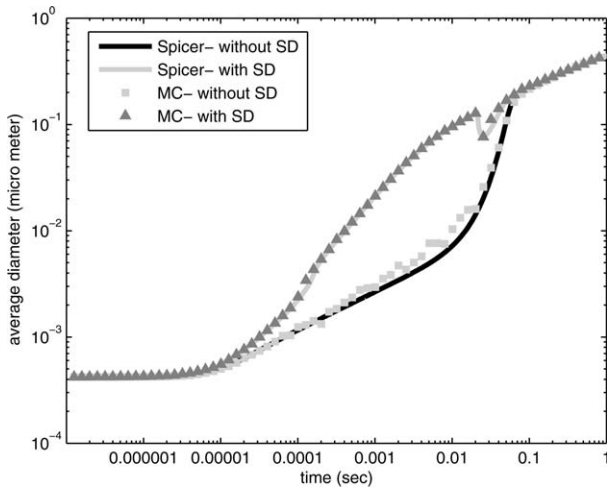


**Figure 3. Size as a function of time with and without surface deposition ($T$ = 1800 K, $x_{TiCl_4}$ = 0.1).**

Size (average diameter) is calculated as the diameter of the average sample rather than the average of all particles diameter to be compatible with Spicer et al.[16] The results of Spicer et al. are also shown for comparison.

the total number concentration. When surface deposition is present, nucleation is limited to a short initial period ($t < 10^{-4}$) during which time the size distribution is wide and approximately a logarithmic function of size. After this point the distribution reaches the characteristic shape due to coagulation. Even though deposition remains active until about $t \approx 0.1$ s, the shape of the size distribution is primarily determined by coagulation, which produces more dramatic changes compared to surface deposition. By contrast, in the absence of surface deposition, the distribution becomes very wide as nucleation produces fine particles and coagulation forms larger ones. Once the gas-phase $TiCl_4$ is depleted, the distribution attains very rapidly the shape that is characteristic of coagulation. This fast transition is fueled by the large coagulation rate between the very small and very large particles in the distribution.

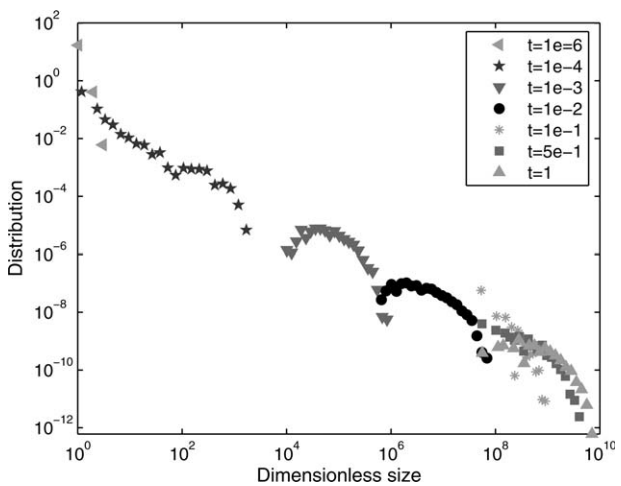


**Figure 4. Size distributions for $T$ = 1800, $x_{TiCl_4}$ = 0.1 with surface deposition included.**

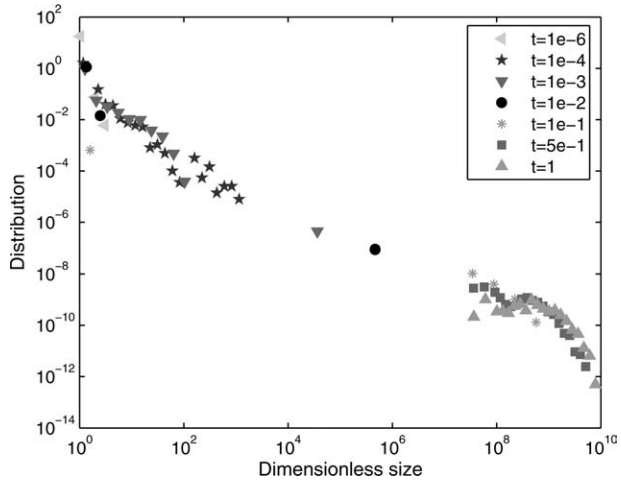


**Figure 5. Size distributions for $T = 1800$, $x_{TiCl_4} = 0.1$ without surface deposition.**

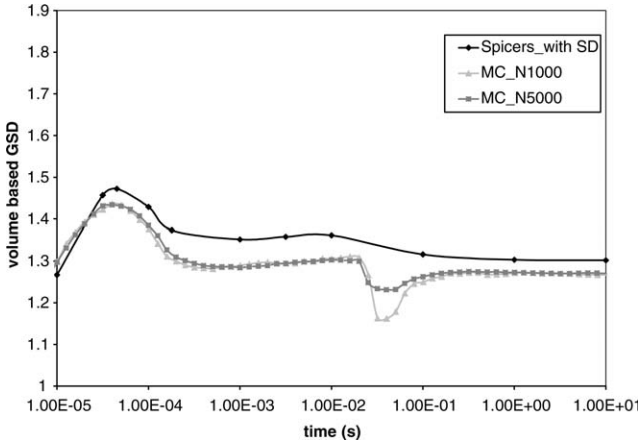


**Figure 7. Volume-based geometric standard deviation (with surface deposition): $T = 1800$ K, $x_{TiCl_4} = 0.1$.**

Some moments of interest are shown in Figure 6 for the case that includes surface deposition. The mass concentration of particles increases until all of the gas-phase $TiCl_4$ is exhausted at which point the mass concentration is 1. We note that the mass balance is strictly obeyed because it is built into the equations for $c_M$ (Eq. 23) and $c_0$ (Eq. 25). Also shown is the average area per particle, $\overline{a}$, and the total surface area, $a = c_p\overline{a}$, both showing a peak corresponding to the second nucleation burst.

As a further comparison we have calculated the geometric standard deviation, shown in figures 7 and 8 for the case with and without surface deposition, respectively. The geometric standard deviation increases initially, as nucleation and coagulation together produce a wide distribution that stretches from nuclei up to much larger aggregates. Once nucleation ceases and the distribution coalesces to that for coagulation, the standard deviation approaches the asymptotic value for coagulation. We note that the MC method produces a lower value of the standard deviation in both cases but most notably in the absence of surface deposition. This is a consequence of the very high nucleation rate: the simulation box is nearly flooded by nuclei and small particles at the expense of larger aggregates. Since the total number of particles in the simulation box is kept constant, the overabundance of nucleus-size particles is accompanied with a reduction in the accuracy of the size distribution at the high end. This accuracy recovers very quickly once nucleation stops.

*Coarsening.* Previously, the deposition event was defined as the addition of mass $v_D$ to a particle in the simulation box. The value of $v_D$ has been intentionally left unspecified. If the value of $v_D$ is set to the smallest possible value, $v_D = 1$, the simulation approaches the limit of continuous mass deposition but this is done at the expense of execution time since the deposition of a single molecule advances the simulation by a very small amount. By allowing $v_D$ to be larger than 1, the simulation can proceed faster. We refer to this as "coarsening" because it decreases the resolution of the physical process.

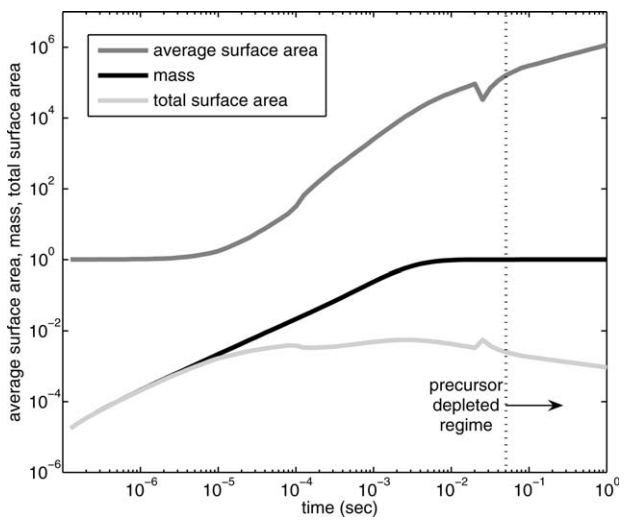


**Figure 6. Average surface area, aerosol mass, and total surface area ($T = 1800$ K, $x_{TiCl_4} = 0.1$).**

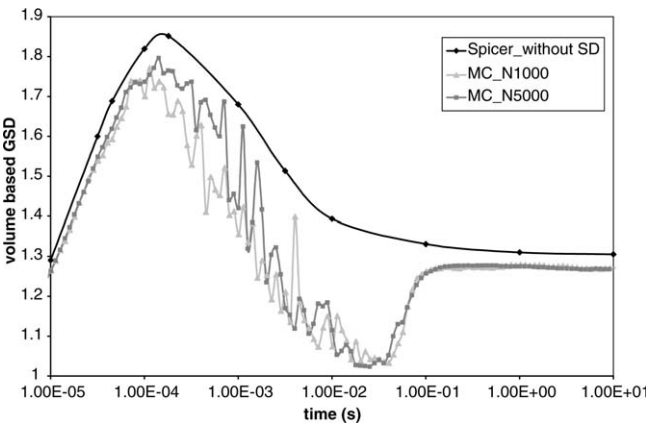


**Figure 8. Volume-based geometric standard deviation (with no surface deposition): $T = 1800$ K, $x_{TiCl_4} = 0.1$.**

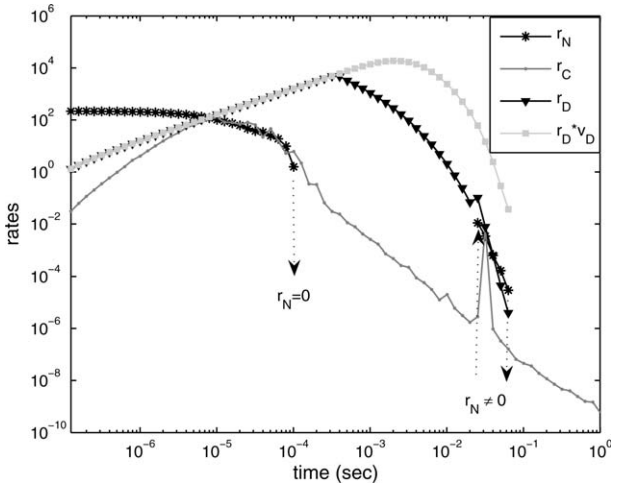


**Figure 9. Rate of events at $T$ = 1800 K, $x_{TiCl_4}$ = 0.1.**

The coarsened deposition rate is $r_D$; $r_D v_D$ is the rate of mass deposition and is equal to the deposition rate without coarsening.

The proper use of coarsening is to accelerate the implementation of the fastest process in the system. If the rate of deposition is the most probable event, then a sizable part of the computation is consumed in calculating event probabilities, even though deposition is the most likely event, and then advance time by a small amount only. By increasing the value of $v_D$, deposition is selected less often but the mass deposited each time is larger with the benefit of advancing time by a larger increment. Note that coarsening does not violate the actual rate at which mass is added to the simulation box: this rate is equal to $r_D v_D$, which is easily confirmed to be independent of the selection of $v_D$ once Eqs. 12 and 13 are taken into account. There is a small loss of accuracy due to the fact that in coarsening the rate of surface deposition we deposit a mass $v_D$ onto a single particle rather than a unit mass onto $v_D$ particles. This error is insubstantial when coagulation is present since coagulation produces much more drastic changes in the size distribution compared to deposition. However, $v_D$ may not be increased arbitrarily. The maximum value of $v_D$ is limited by the requirement that coarsening may only be applied to the fastest process. Accordingly, the coarsened deposition may not become slower than the next slower process. For more discussion on simulation acceleration, see.[24,25]

In these simulations the value of $v_D$ was variable in the simulation according to

$$v_D = \max\{1, (0.0001) \times \bar{v}\}, \tag{28}$$

which adjusts $v_D$ in proportion to the mean mass while setting the minimum value of $v_D$ to 1. According to this rule, $v_D$ is equal to 1 when the simulation consists of small particles, and is gradually increased as the particles grow to larger size. The effect on the rate of deposition is shown in Figure 9 for $T$ = 1800 K, $x_{TiCl_4} = 0.1$ with all three mechanisms included. The coarsened deposition rate implemented in the simulation is denoted by $r_D$ while $r_D v_D$ refers to the noncoarsened rate, also equal to the rate of mass deposition onto the surface of the aerosol. As we see, after approximately $t = 10^{-5}$ s deposition becomes the fastest process; when coarsening is implemented, starting at about $t = 3.2 \times 10^{-4}$ s, the deposition is reduced but even in coarsened formed it remains the fastest rate. This gives confidence that accuracy is not compromised, a conclusion that is confirmed directly by the excellent agreement with the simulations of Spicer et al.[16] in Figure 3.

*Other numerical bottlenecks.* Simulations become considerably slower when surface deposition is not included (see run times in Table 3). This is because the benefit of coarsening is now lost. While coarsening may in principle be used on nucleation, this is inappropriate under the conditions of our runs because nucleation is the rate-limiting process and has a significant effect on the particle size distribution. This is demonstrated in Figure 10 which shows the rate of nucleation and coagulation in the absence of surface deposition. Initially, nucleation is the only active process. Once the concentration of particles increases sufficiently, the coagulation rate increases but it never exceeds the rate of nucleation – at most, the two rates are equal, until the concentration of $TiCl_4$ is exhausted. The physical reason for this behavior is the fact that the coagulation kernel is highest between the smallest and largest particles. As nuclei are formed, they are immediately consumed by coagulation, whose rate falls as a result of the depletion of the number concentration leaving the process waiting for the next nucleation event. This is clearly demonstrated by the time constants of nucleation and coagulation in Table 3. Though a small degree of coarsening in the form of adding $n > 1$ nuclei per nucleation event may be tolerated, the effect on the size distribution could be important given the sensitivity of coagulation to the relative amounts of small and large particles.

A further consequence of quasi-steady state that is established by the competing rates of nucleation and coagulation (Fig. 10) is the presence of fluctuations in the mean particle size. The generation of new particles by nucleation decreases the mean size but the presence of small and large particles fuels the rate of coagulation, causing the size to drop. These fluctuations are visible in Figure 3 in the form of noise in the MC results when compared to the results of the sectional

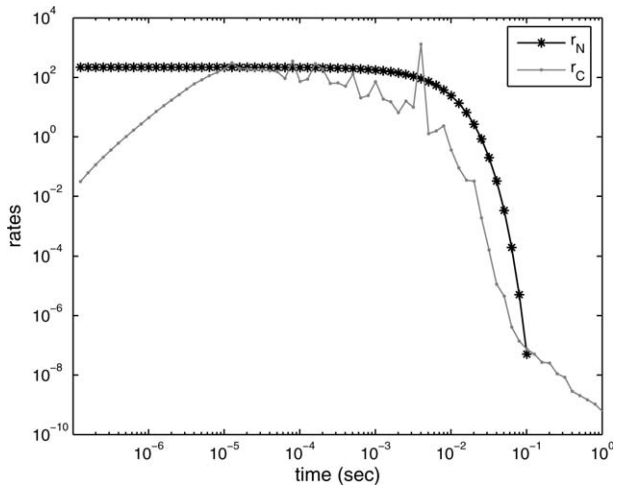


**Figure 10. Nucleation and coagulation rate in the absence of surface deposition ($T$ = 1800 K, $x_{TiCl_4}$ = 0.1).**

method in the absence of surface deposition. In this region, size fluctuations may be as high as 30% but they drop to less than 2% when the precursor is depleted and the system is driven solely by coagulation.

## Conclusions

In summary, we have shown that constant-number MC can be extended to problems involving population balances with various interacting processes. Additional processes such as flow in and out via streams, evaporation/dissolution, etc. can be added easily by updating Eq. 24 as to the effect of these processes on the mass of the simulation box. Sintering can also be incorporated. This, however, requires some additional effort because the population balance in this case becomes bivariate as the particle surface must be treated as independent variable in addition to particle mass. This extension will be considered in the future. The main conclusion of the present work is that kinetic MC can serve as a complete environment for the simulation of particulate processes under realistic conditions, and that sufficient accuracy can be maintained with a rather small number of simulation particles, well within the capabilities of desktop computing.

## Acknowledgments

This study is based upon work partially supported by the National Science Foundation under Grant #CBET-0651644 (Matsoukas) and CAREER Award #CBET 06-44519 (Armaou).

## Literature Cited

1. Haseltine EL, Patience DB, Rawlings JB. On the stochastic simulation of particulate systems. *Chem Eng Sci*. 2005;60:2627–2641.
2. Kumar S, Ramkrishna D. On the solution of population balance equations by discretization–iii. nucleation, growth and aggregation of particles. *Chem Eng Sci*. 1997;52:4659–4679.
3. Immanuel CD, Doyle FD. Computationally efficient solution of population balance models incorporating nucleation, growth and coagulation: application to emulsion polymerization. *Chem Eng Sci*. 2003;58:3681–3698.
4. Maisels A, Kruis FE, Fissan H. Direct simulation Monte Carlo for simultaneous nucleation, coagulation, and surface growth in dispersed systems. *Chem Eng Sci*. 2004;59:2231–2239.
5. Celnik M, Patterson R, Kraft M, Wagner W. A predictor-corrector algorithm for the coupling of stiff ODEs to a particle population balance. *J Comp Phys*. 2009;228:2758–2769.
6. Raj A, Celnik M, Shirley R, Sander M, Patterson R, West R, Kraft M. A statistical approach to develop a detailed soot growth model using PAH characteristics. *Combustion Flame*. 2009;156:896–913.
7. Mosbach S, Celnik MS, Raj A, Kraft M, Zhang HR, Kubo S, Kim K. Towards a detailed soot model for internal combustion engines. *Combustion Flame*. 2009;156:1156–1165.
8. Hounslow MJ, Ryall RL, Marshall VR. A discretized population balance for nucleation, growth, and aggregation. *AIChE J*. 1988;34:1821–1832.
9. Christofides PD, El-Farra N, Li M, Mhaskar P. Model-based control of particulate processes. *Chem Eng Sci*. 2008;63:1156–1172.
10. Dokucu MT, Park M, Doyle FJ. Reduced-order methodologies for feedback control of particle size distribution in semi-batch emulsion copolymerization. *Chem Eng Sci*. 2008;63:1230–1245.
11. Li M, Christofides PD. Computational study of particle in-flight behavior in the HVOF thermal spray process. *Chem Eng Sci*. 2006;61:6540–6552.
12. White CM, Zeininger G, Ege P, Ydstie BE. Multi-scale modeling and constrained sensitivity analysis of particulate CVD systems. *Chem Vapor Deposition*. 2007;13:507–512.
13. Christofides PD, Li M, Madler L. Control of particulate processes: recent results and future challenges. *Powder Technol*. 2007;175:1–7.
14. Kiparissides C. Challenges in particulate polymerization reactor modeling and optimization: a population balance perspective. *J Process Control*. 2006;16:205–224.
15. Irizarry R. Fast Monte Carlo methodology for multivariate particulate systems-I: point ensemble Monte Carlo. *Chem Eng Sci*. 2008;63:95–110.
16. Spicer PT, Chaoul O, Tsantilis S, Pratsinis SE. Titania formation by $TiCl_4$ gas phase oxidation, surface growth and coagulation. *J Aerosol Sci*. 2002;33:17–34.
17. Tsantilis S, Kammler HK, Pratsinis SE. Population balance modeling of flame synthesis of titania nanoparticles. *Chem Eng Sci*. 2002;57:2139–2156.
18. Mühlenweg H, Gutscha A, Schilda A, Pratsinis SE. Process simulation of gas-to-particle-synthesis via population balances: Investigation of three models. *Chem Eng Sci*. 2002;57:2305–2322.
19. Tsantilis S, Pratsinis SE. Evolution of primary and aggregate particle size distributions by coagulation and sintering. *AIChE J*. 2000;46:407–415.
20. Pratsinis SE, Spicer PT. Competition between gas phase and surface oxidation of $TiCl_4$ during synthesis of $TiO_2$ particles. *Chem Eng Sci*. 1998;53:1861–1868.
21. Seinfeld JH, Pandis SN. *Atmospheric Chemistry and Physics*. Wiley, New York, 1998.
22. Smith M, Matsoukas T. Constant-number Monte Carlo simulation of population balances. *Chem Eng Sci*. 1998;53:1777–1786.
23. Lin Y, Lee K, Matsoukas T. Solution of the population balance equation using constant-number Monte Carlo. *Chem Eng Sci*. 2002;57:2241–2252.
24. Gillespie DT. Approximate accelerated stochastic simulation of chemically reacting systems. *J Chem Phys*. 2001;115:1716–1733.
25. Gillespie DT, Petzold LR. Improved leap-size selection for accelerated stochastic simulation. *J Chem Phys*. 2003;119:8229–8234.

## Appendix

### *Coagulation kernel*

We write Fuchs' interpolation formula[21] for the coagulation kernel in the form

$$K_{12} = K_0 k_{12} \tag{A1}$$

such that $K_0$ is the dimensional part of the kernel ($m^3/s$) and $k_{12}$ is a dimensionless function of the size of the coagulating particles. This separation of dimensions is done using the titania molecule as the basis for defining a set of characteristic dimensional quantities:

$$R_* = 2.1 \times 10^{-10}\ \text{m} \tag{A2}$$

$$M_* = \frac{4\rho\pi R_0^3}{3} = 1.5517 \times 10^{-25}\ \text{kg} \tag{A3}$$

$$D_* = \frac{k_B T}{6\pi\mu R_0} \tag{A4}$$

$$V_* = \left(\frac{k_B T}{8\pi M_0}\right)^{1/2} \tag{A5}$$

Variables $R_*$, $M_*$, $D_*$, and $V_*$ represent a characteristic length, mass, continuum diffusivity, and mean thermal velocity, respectively. The numerical values for $R_0$ and $\rho = 4000\ \text{kg/m}^3$ are taken from ref.[16] The dimensional part of the kernel is

$$K_0 = 4\pi D_* R_* \tag{A6}$$

The dimensionless part is given as a function of the dimensionless radius $r_i = R_i/R_0$ of the coagulating particles,

$$k_{12} = \frac{r_1 + r_2}{\beta_{12} + \gamma_{12}} \left( \frac{\alpha_1}{r_1} + \frac{\alpha_2}{r_2} \right) \tag{A7}$$

where:

$$\alpha_i = \frac{5 + 4Kn_i + 6Kn_i^2 + 18Kn_i^3}{5 - Kn_i + (8 + \pi)Kn_i^2} \tag{A8}$$

$$\beta_{12} = \frac{r_1 + r_2}{r_1 + r_2 + \sqrt{r_1^2\phi_1^2 + r_2^2\phi_2^2}} \tag{A9}$$

$$\gamma_{12} = \frac{A(\alpha_1/r_1 + \alpha_2/r_2)}{(r_1 + r_2)\sqrt{1/r_1^3 + 1/r_2^3)}} \tag{A10}$$

$$\phi_i = \frac{(\kappa_i + 2)^3 - (\kappa_i^2 + 4)^{3/2}}{6\kappa_i} - 2 \tag{A11}$$

$$\kappa_i = \frac{B\alpha_i}{\sqrt{r_i}} \tag{A12}$$

$$A = 4D_*/R_*V_* \tag{A13}$$

$$B = 8D_*/\pi R_0 V_* \tag{A14}$$

In the above, $Kn_i = R_i/\lambda_g$ is the Knudsen number of the particles, with the mean free path of the gas calculated as

$$\frac{\lambda_g}{m} = 6.86 \times 10^{-8} \left( \frac{\text{bar}}{P} \right) \left( \frac{T}{298\,\text{K}} \right) \tag{A15}$$

*Manuscript received Aug. 27, 2009, revision received Dec. 18, 2009, and final revision received Feb. 22, 2010.*